DYNAMICS OF SHEAR THICKENING FLUIDS IN COMPOSITE BEAM STRUCTURES

by

James McGovern

A thesis submitted to the Faculty of the University of Delaware in partial fulfillment of the requirements for the degree of Bachelors in Chemical Engineering.

Spring 2010

DYNAMICS OF SHEAR THICKENING FLUIDS IN

COMPOSITE BEAM STRUCTURES

by

James McGovern

Approved: _____

Norman Wagner, Ph.D.
Professor in charge of thesis on behalf of the Advisory Committee

Approved: _____

John Gillespie, Ph.D.
Committee member from the Department of Mechanical Engineering

Approved: _____

Susan Groh, Ph.D.
Committee member from the Board of Senior Thesis Readers

Approved: _____

Ismat Shah, Ph.D.
Chair of the University Committee on Student and Faculty Honors

TABLE OF CONTENTS

LIST OF TABLES

LIST OF FIGURES

ABSTRACT

The next generation of armored vehicles will have to face a host of ever more lethal weapons platforms designed specifically to defeat armor plating. As weapons technology advances, traditional steel armors are quickly becoming obsolete. New armor systems have shifted to the use of high strength composites and ceramics. Unfortunately, these ceramics are brittle, and can become damaged merely by driving. Damage can be mitigated with a compliant interlayer between the armor plate and vehicle frame. However, this will reduce the overall protection from ballistic threats.

Shear Thickening Fluids (STFs) have been proposed as a novel interlayer material. STFs can be engineered to remain liquid-like and fluid during vehicle mobility. Once struck by a high energy, high shear rate projectile, the STF will nearly instantly transform into a rigid solid-like state, effectively binding the armor and frame together and improving performance.

Computer modeling of the dynamics of the interlayer system under various velocity profiles has shown the systems are highly sensitive to both the deformation rate, as well as the shape of the deformation rate v deformation curve. In particular, sinusoidal rates such as those generated by a dynamic mechanical analyzer cause viscous forces to dominate, while those similar to ballistic impacts stress elastic forces.

The computer results were compared to experimental data with mixed results. The models were found to predict some features, but overestimate others. Further experimentation will be required to eliminate any possible systematic error in the experimental results before the simulations can be confirmed or denied.

Chapter 1

INTRODUCTION

1.1 Shear Thickening Fluids

Shear Thickening Fluids (STFs) are a novel class of non-Newtonian fluids that have been the subject of extensive current research due to their applications in personal body armor and protective gear [16]. These fluids have a unique rheology where, unlike Newtonian fluids for which the viscosity can be described by one fixed value, and the fluids resistance is merely proportional to how quickly it is being forced to flow, STFs have a highly non-linear viscosity depending on the shear rate. Typically, when starting from rest, the fluid will initially thin with increasing shear rate, but at a critically point will begin to thicken until, in many cases, it will resemble a rigid solid. This transition can be nearly instantaneous, in which case it is a discontinuous STF, or can occur gradually with increasing shear rate (a continuous STF).

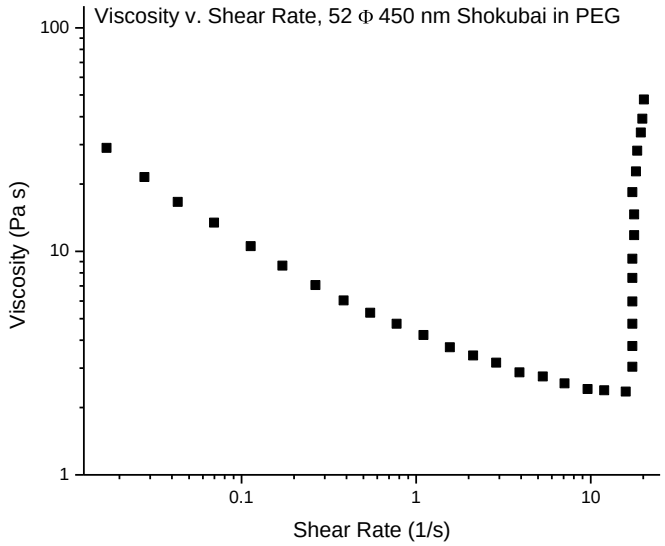

Figure 1.1-Viscosity plotted against shear rate for a discontinuously shear thickening STF.

STFs are highly concentrated suspensions of colloidal particles dispersed in a liquid base. Virtually any material can be used as the solid phase, with ceramics such as silica and aluminosilicates being common. Many different particle geometries have been successfully employed, with particle sizes ranging from tens of nanometers up to over a micron. Often, the particles are also surface treated to promote stability in high volume fractions used in many STFs, which can be greater than 60%. The liquid bases employed are generally non-volatile, to increase the service life of the suspension, but more importantly must be chosen such that a stable suspension is formed with the particle system. Typical fluids are low molecular weight polymers such as poly-ethylene glycol, poly-propylene glycol, and mineral oil.

At rest, the suspended particles in an STF are in equilibrium, with all of the particles randomly moving due to Brownian motion. As shear is applied to the sample, the particles will begin to flow in a controlled and ordered fashion, essentially flowing in low resistance lanes along streamlines. This leads to the shear thinning phenomena, due to minimal interactions between the flowing particles. As the shear rate increases, however, the forces making the particles flow overcomes the thermodynamic forces keeping the particles apart, and large hydroclusters form [8]. These hydroclusters exhibit a much higher resistance to flow than the individual particles. This manifests as a many order of magnitude increase in viscosity. Once the shear forces are removed from the sample, the thermodynamic forces such as Brownian motion redisperse the particles, and the viscosity returns to original levels.

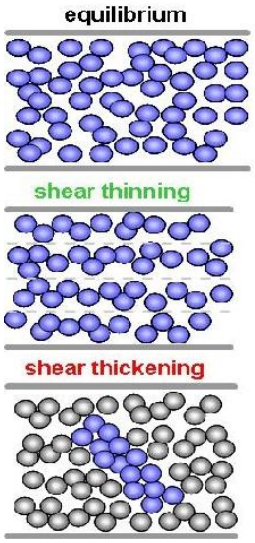

Figure 1.2-Cartoon conceptualization of the shear thickening phenomenon.

1.2 STF Body Armor

One of the most promising applications for STFs is in the field of personal protective equipment for everything from sports attire to medical gloves to ballistic vests. When STF is added to a woven fabric, the result is a material that maintains the flexibility of the original fabric, while drastically increasing its resistance to puncture and cut from a vast variety of threats [9]. Normally, the coating process adds about 20% more areal density to the fabric. However, the added protection is much more than can be achieved by adding an equivalent number of fabric layers, resulting in a net weight reduction in order to defeat a given threat. Further the composite has increased mobility due to fewer fabric layers and a resulting more compliant garment.

STF is added to the fabrics using a simple dip coating process. A volatile dilutant, such as ethanol, is added to the STF in order to reduce its viscosity and prevent it from shear thickening, both of which must be accomplished in order to make the suspension workable. The fabric to be treated is then soaked in diluted STF, and ample time is allowed for the suspension to work itself into the weave of the cloth. Once thoroughly saturated, the fabric is removed from liquid, and excess STF is squeezed out using a roll press. Finally, the fabric is hung up and the ethanol carrier allowed to evaporate. The result is a fabric which has been intimately saturated with the shear thickening fluid. The fluid has coated the individual yarns and filaments, in particularly at the junctions of two crossed yarns, where troughs are formed for the STF to pool into.

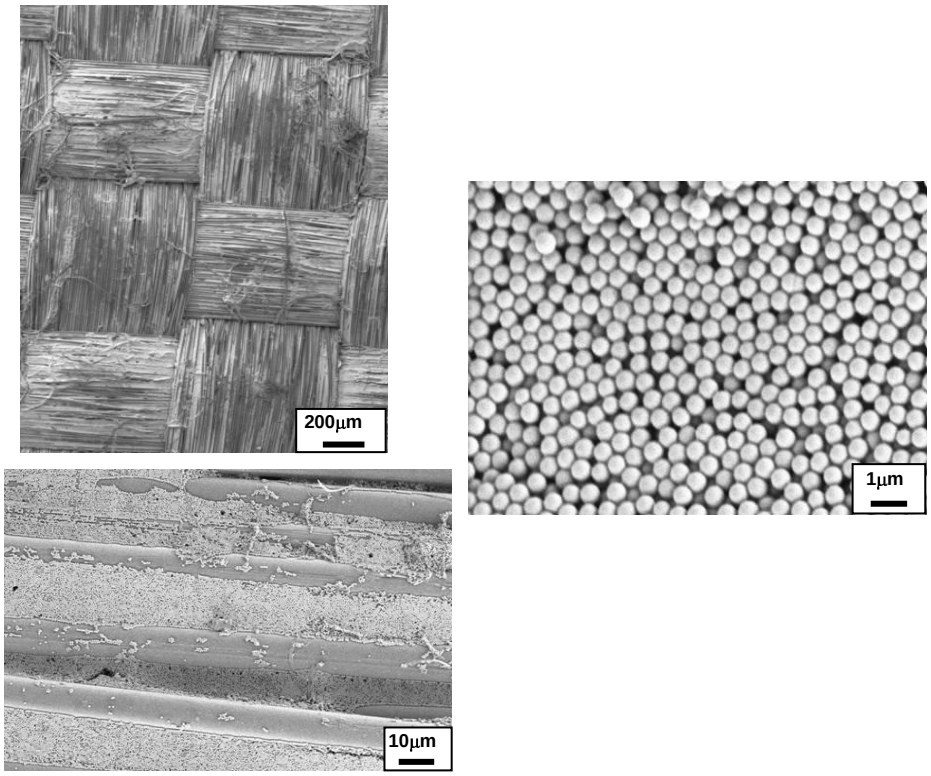

Figure 1.3-Electron microscopy images of Shokubai nanoparticles coating Kevlar yarns. [16]

STF treated fabrics fold and flex as freely as the original, untreated fabric. This is because folding and flexing causes very little relative movement between the individual yarns in the fabric. Rather, the entire sample deforms as a whole, and relatively minor amounts of stress is transmitted to the fluid. However, during high energy impacts, such as a ballistic event, this is not the case. When a projectile engages an untreated sample, it does not engage the entire area of the fabric. Rather, only the few yarns directly intersecting the path of the projectile are directly engaged. These yarns begin to slide out of the weave, in order to create a pocket underneath the projectile, and continue to pull out until there is enough room for the object to slip in between the yarns,

a phenomenon called windowing [11]. During this event, the remainder of the fabric has only one job: to provide friction to the engaged yarns, thus slowing the projectile. When an identical projectile is incident upon a treated fabric, initially, the engaged yarns attempt to pull out similar to the untreated fabric. However, this causes a large amount of shear to be applied to the STF coating the yarns and filling the junctions, which will nearly instantaneously transition to its solid-like state, and prevent further pull out [12]. This causes the impact forces and energy to be transferred to neighboring yarns, engaging the entire sample rather than just the incident yarns. Essentially, the impact site is allowed to "borrow" strength from the rest of the fabric, and traditional failure mechanisms such as windowing are essentially prevented.

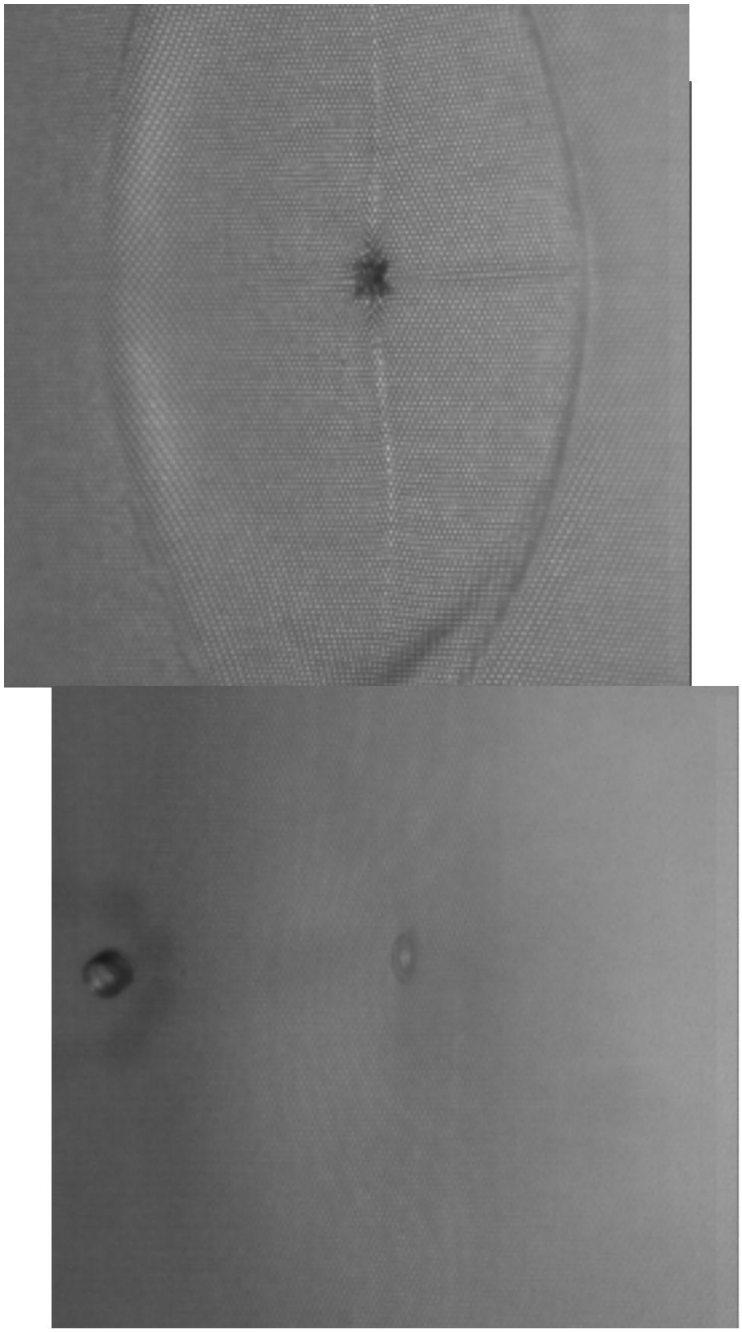

Figure 1.4-Comparison of ballistic tests performed on neat (top) and STF treated (bottom) samples of ballistic nylon. Note the perpendicular cross in the neat sample, caused by pullout of the immediately affected yarns. No such damage is evident in the STF treated fabric. [15]

1.3 Composite Vehicle Armor

Over the past several years, composite vehicle armor has been garnering significant attention, as it theoretically offers several important advantages over traditional armor technologies, such as rolled homogeneous or reactive armor. Composite armor systems tend to be lighter than steel alternatives for the same level of protection, thus allowing adoption on smaller vehicles with high mobility requirements. More importantly, however, these armors offer exceptional protection against the latest generation of shaped charges as well as kinetic energy penetrators.

Composite armor is composed of several distinct materials bonded together. They all utilize a toughened strike face, typically composed of a high strength ceramic, and can exist as discrete plates, inside of a metal matrix, or can even be cast as a monolithic shell. This strike face is bonded, through the use of an elastic interlayer material, to the frame of the vehicle. [4] Further, other components may exist, such as extra layers composed of resin-impregnated ballistic fabrics, void spaces or metals, added to improve the physical properties, and hence protective rating, of the composite structure.

Although offering minimal protection itself, the bonding agent has a role in the composite system that is more than simply binding the different layers together. The interlayer acts as a medium through which the stresses are transferred from the strike face to the vehicle frame and vice versa. As such, it can be tailored to one of the two loads experienced by the vehicle over its service life. Mobility loads are a result of vehicle traveling over uneven terrain. Every bump and pothole will cause low energy, low frequency vibrations throughout the structure of the vehicle. These vibrations are

particularly harmful to the brittle ceramics that form the armor face. Over time, the damage accumulates as micro cracks form, and the protective rating of the armors decreases, until they are no longer effective and must be replaced. For this type of load, a compliant, rubbery adhesive interlayer is desirable. It will allow for limited relative motion between the strike plates and frame, simultaneously insulating the plates and dampening the vibrations. Such a setup will allow for a longer service life for the armor components, and decrease down time, material costs, support crew, and logistics.

On the other hand, during a ballistic event, a rubbery compliant interlayer is not desirable. During a high energy, high strain rate ballistic load, a hard, rigid interface is superior. In this case, having the frame and strike face firmly bonded together and acting as a unit will result in a higher performance and more protection than allowing the frame and strike plates to operate as two distinct entities. Ultimately, the properties that make an interlayer favorable for one of the loads will decrease performance when subject to the other kind. With simple elastic interlayers, it is impossible to design a system that will perform as desired under all conditions.

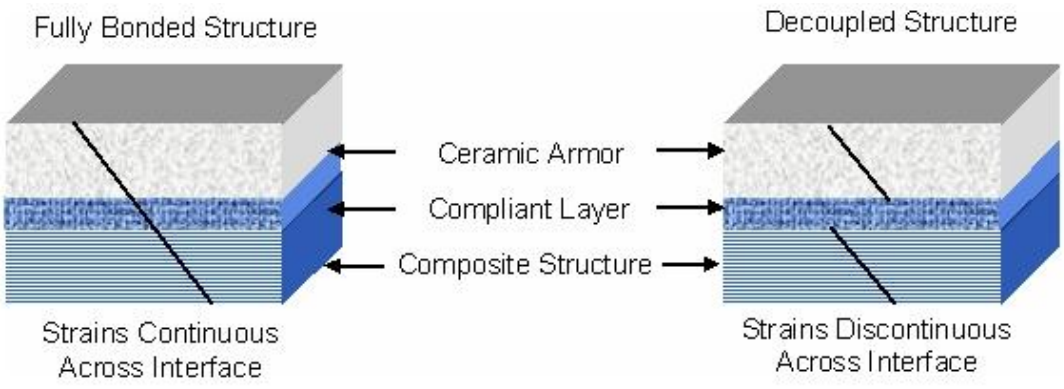

Figure 1.4-Comparison of strains in armor systems with rigid and flexible interlayers.

The purpose of this project was to examine the possibility of utilizing shear thickening fluids as a novel interlayer material that can perform under both sets of loads. Such an STF would be engineered to be in the low viscosity/ shear thinning regime for the low amplitude mobility loads, effectively decoupling the armor plating from the vehicle frame. However, under the high deformation rates characteristic of ballistic loads, the STF would reactively thicken into its solid state, thereby rigidly coupling the armor and frame for improved protection. The same properties that make STFs desirable for personal body armor also make it desirable for vehicle armor applications. Namely, it is fluid and allows for motion under normal conditions, but becomes solid and unyielding when struck by a projectile.

Testing was limited to a nondestructive examination of the properties of the interlayer when subject to varying strain rates. As a surrogate for the armor system, a simplified composite beam of a thin layer of interlayer material sandwiched between two uniform polymer beams was used. This system was subjected to a 3 point bend test at varying velocities, with each velocity generating a different shear rate in the interlayer adhered. Modeling was carrying out using analytical beam bending models modified for the viscous nature of the interlayer. Laboratory level experiments were performed on a Mettler Toledo DMA (Dynamic mechanical analyzer), set up in a three point bend mode. Finally, the knowledge gained from these experiments was used to develop an experiment for the “Tower of Power”, a 12 foot tall drop tower capable of replicating the energies of a modern combat rifle round.

Chapter 2

THREE POINT BEAM BENDING

2.1 Previous Experiments

A 2006 paper by Fischer et al. detailed a study of viscous interlayer sandwich beams. The main focus was on engineering the dampening coefficient of the beam system through the addition of a field responsive material, such as an STF. [7] Ultimately, they demonstrated that STF were able to modify both the stiffness and dampening of the beams under dynamic bending.

The Fischer experiment employed a cantilever setup. The beam was clamped at one end, with the other unsupported. An actuator would drive the unsupported end, while a laser measured its displacement. By measuring the stready state displacement, as well as the amount of force required to maintain the oscillations, important beam parameters could be back calculated, including the stiffness and dampening coefficient.

The beams used were composed of polyvinyl chloride, and were approximately 150mm long by 40mm wide, and either 2 or 6 mm thick. The interlayer was held to either 85 or 140 µm by the addition of a small amount of nylon fibers.

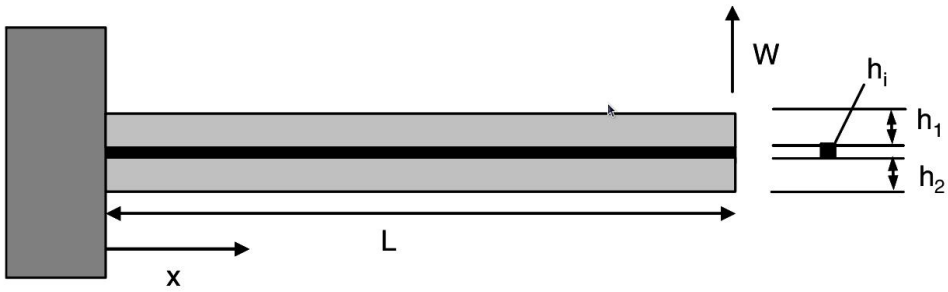

Figure 2.1-Diagram of Fischer's cantilever experiment.

In one experiment, in which a silica based STF was used as the interlayer material, it was demonstrated that above a critical displacement, the dampening of the beam oscillations increased significantly. This was attributed to the relative motion of the beams causing a shear thickening transition in the interlayer. The increased viscosity resulted in a dramatic increase in viscous dissipation, ultimately dampening the beam.

In a second experiment, the STF interlayer was instead replaced with a slow curing epoxy, which would slowly increase in viscosity over approximately 8 hours, before fully crosslinking. Over approximately the first decade in interlayer viscosity (1 through 10 Pa s), little change was observed in the mechanics of the beam. However, over the next few decades, the dampening coefficient began to increase as the viscous interlayer forces became important. Finally, as the epoxy approached its final state and the viscosity became increasingly enormous, the increase in dampening died out, but the beam stiffness increased drastically, as the beams became bonded together.

In a second paper released in 2010, the Fischer group expanded upon their original research, investigating the effect of the rheological properties of the STF in

respect to the overall beam properties. [6] Several varieties of STF were used, in the same experimental setup from the 2006 paper. Further, the results were compared, with good agreement to a computer based model.

The computer simulation is a finite element analysis based upon the Timoshenko method [6], because the shear is critically important to the model. The model solves for shears and strains throughout the beam as a function of displacement and frequency based on a matrix of beam properties, such as the storage and loss modulus. An iterative loop was also required to ensure the interlayer STF complex viscosity based upon the shear rate returned from the model matched the STF properties used as an input.

The model was able to demonstrate that the STF properties had a large impact upon the final beam properties. Both of the STFs modeled resulted in both a stiffness and dampening increase with increasing displacement and velocity. However, the magnitudes of the increases, as well as the resonant frequency varied greatly depending upon which STF was considered.

2.2 Gillespie Sandwich Beam Model

Design of the experiments was influenced heavily by an analytical beam bending model developed by Gillespie et al [1]. The model solves for the compliance of a purely elastic composite beam undergoing a three point bend. It solves for beams of identical geometry and (uniform) modulii being subject to small deformations. Sandwiched in between the beams is a layer of elastic adherend, with a finite thickness much less than that of the main beams, and uniform in its properties. The model solves for two distinct cases. The first has no beam overhang; in other words, the beam ends at the grounding supports. The second case allows for overhang.

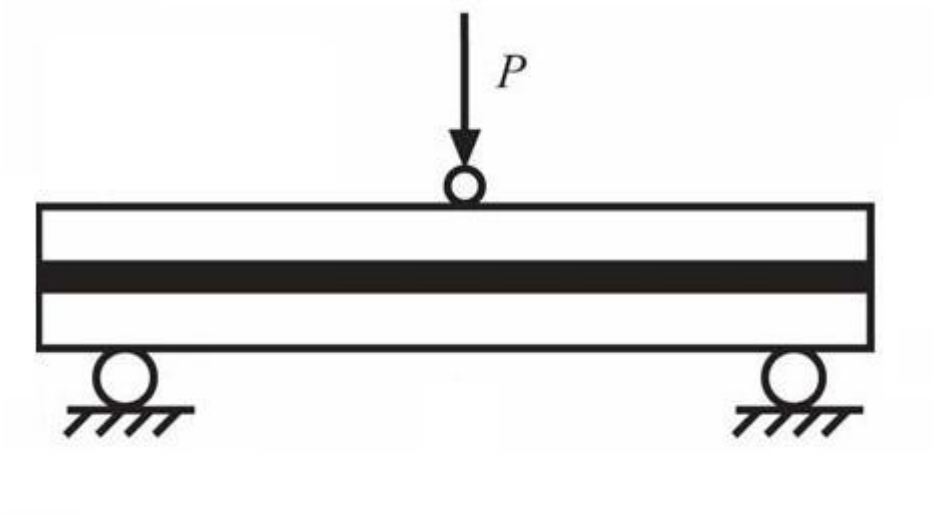

Figure 2.2-Schematic of a three point bend test.

Among the main implications of the model was that the properties of the interlayer have a profound effect on the properties of the beam as a whole. For beams with an interlayer material of infinitesimal modulus, the beams are essentially decoupled, and as such the system is very compliant. As the modulus of the interlayer increases, however, the compliance falls until the interlayer modulus is identical to the beam modulus. At this point, the compliance is about 1/2 the compliance of the unbonded beams. Further increases in interlayer modulus beyond this point will continue to marginally decrease the beam's compliance.

The model can also solve for the mechanical stresses and strains experienced by the composite structure as a result of the displacement load. Of particular interest to this project is the shear in the interlayer. It is fairly simple to back this value out (as a function of the position along the beam). This value can then be

differentiated with respect to time to find the shear rate, the defining property when the model is expanded to include viscous interlayers.

The interlayer shear as a function of displacement takes up an interesting shape. For beams without overhang, at the edges of the beams the shear is at a maximum. The center of the beam is approached, the shear decays with the hyperbolic cosine, until at the center point of the beam, there is a cusp with zero shear. As one moves farther down the length of the beam away from the center and towards the far edge, the shear once again grows as the mirror image. The implications of this shape for viscous and shear thickening interlayers is important. First, only the tips of the beams will be contributing to viscous dissipation of energy. Secondly, only a portion of the STF will be above the critical shear rate. As the center is approached, the shear rate will never be high enough to thicken the sample regardless of displacement rate.

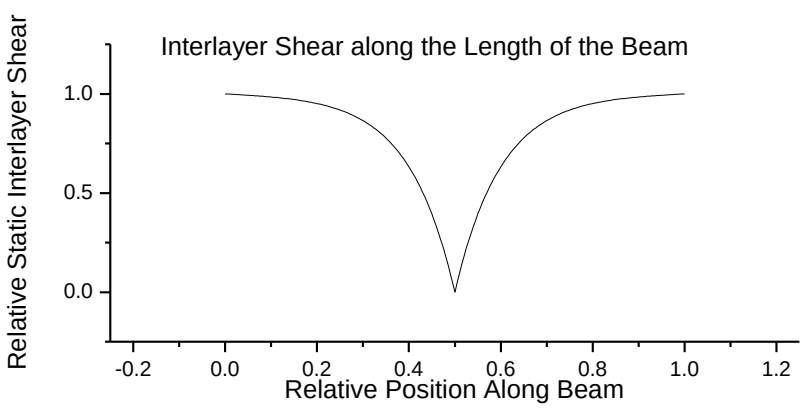

Figure 2.3-Shear in the interlayer as a function of position along the beam. This is a representative curve. The exact shape may change depending upon the beam geometry and materials.

2.3 Overview of Experiments

As opposed to the cantilever beam experiments undertaken by the Fisher group, all of the experiments herein utilize three point bend geometry, such as the one solved for by Gillespie. In a three point bend, both ends of the beam are supported (not clamped), typically by resting the beam on two pillars. An actuator forces the beam to deflect in the middle of the two supports, causing to roughly conform to a V shape. The bending modulus, and hence the energy required to bend the beam a set distance is heavily dependant upon not only the elastic modulus of the beam, but also the distance of the support span, and the thickness of the beam. Wider beams are easier to deflect, while thicker ones are many times more difficult.

The three point bend geometry was chosen because it more closely resembles a vehicle being struck by a single projectile than the cantilever geometry used by Fischer. Vehicles are constructed with rigid posts, such as those between the windows of cars, with a skin; sheet metal in a car, armor plates in military vehicle; spanning the posts. During a ballistic impact, the posts would act somewhat like the in the three point bend, with the projectile causing the armor to deflect at some arbitrary point in between two of the posts.

Three individual experiments were undertaken studying the system. First, a computer model was developed. This provided a background for understanding the underlying physics, and provided a point of reference for the design of the DMA experiments. The DMA experiments involved subjecting physical beams with differing interlayers to variable deformation rates. These results were compared to the computer models. Any disagreements were corrected by modifying the code to reflect a more realistic scenario. Finally, the third experiment was a computer based prediction of the results for a “Tower of Power” (a new high energy drop tower at the University of

Delaware's Center for Composites Manufacture) experiment on an STF sandwich beam.

The initial computer model is based upon the Gillespie analytical sandwich beam model. The model was modified to solve for the shear rate in the interlayer as a dynamic quantity, as opposed to the static properties, such as interlayer shear, used in the original solution. This allows the calculation of the viscous interactions occurring in the interlayer, as well as an effective elastic modulus for the otherwise purely viscous interlayer, by comparing the wall stresses generated by the flowing fluid to an elastic interlayer generating identical forces. This ultimately allowed for the study of how the dynamic interlayer properties affected the overall elastic properties of the beam.

Results from the initial modeling were then used to help finalize the beam dimensions for the DMA experiments. Since the DMA generates a sinusoidal input wave, this experiment is very similar to the work performed by the Fischer group, with a periodic, vibrating beam. As such, it was anticipated that the results should be similar, with the STF showing an increase in both stiffness and dampening. Eventually, this was in fact found to be the case.

Finally, the computer model was modified to apply to the drop tower. Unlike the cantilever and DMA test, this is not a periodic experiment, but rather a single deflection. Further, the impact is extremely violent and dynamic. Modeling suggested that under such circumstances, the dampening effect of the STF is secondary and minimal. The main mechanism through which the STF acts in such a case is to reduce the system compliance.

Chapter 3

MODELING THE DMA

3.1 Modification of Gillespie Equations for Viscous Interlayers

Professor Gillespie's beam equations were combined with Newtonian mechanics and fluid dynamics to create several detailed models of sandwich beam composites with viscous interlayers. These models were used to select the parameters for the experimental beams. The models were also compared to the experimental results to validate the underlying mechanical models used to describe the dynamics. All of the models were programmed in MATLAB, using iterative techniques and a finite element approximation.

Modification of the model to include a viscous interlayer relied upon the calculation of the interlayer shear rate. This would allow for the calculation of the viscous forces exerted by the interlayer. However, the Gillespie model does not address dynamic quantities such as shear rate, but rather static ones such as strain. In order to calculate shear rate, several substitutions had to be made, and starts with the compliance. (See Nomenclature section for definitions of all symbols)

$$C = \frac{x}{P} = C_{bt}(1 + \frac{Ah^2}{12D}(1 + \frac{t}{h})^2[\frac{36}{\kappa^2 L^2} - \frac{72}{\kappa^3 L^3} tanh(\frac{\kappa L}{2})])$$

eqn. 3.1

This can be rearranged to solve for the force (P), as a function of the displacement (x). The derivative of the force with respect to time, a quantity very closely related to the jerk, is the only time varying value in the dynamic solution.

$$\frac{dP}{dt} = \frac{d\frac{x}{c}}{dt} = \frac{v}{c}$$

eqn. 3.2

Calculation of the interlayer shear first requires calculation of the interlayer shear stress, which is found through the maximum interlayer shear stress, τ bar.

$$\bar{\tau} = \frac{3}{4}\frac{\bar{V}}{bh}\frac{1+\frac{t}{h}}{1+\frac{3t}{2h}+\frac{3}{4}(\frac{t}{h})^2}$$

eqn. 3.3

The quantity V bar in this expression is related directly to the force.

$$\bar{V} = \frac{P}{2}$$

eqn. 3.4

The only quantity with a time derivative in the expression for the maximum interlayer stress is V bar. The derivative therefore becomes:

$$\dot{\bar{\tau}} = \frac{3}{8}\frac{v}{cbh}\frac{1+\frac{t}{h}}{1+\frac{3t}{2h}+\frac{3}{4}(\frac{t}{h})^2}$$

eqn. 3.5

The maximum interlayer stress is related to the shear stress along the interface along the length of the beam (z) by a function of the hyperbolic cosine. Again, the only quantity in the expression with a time derivative is the maximum interlayer stresss.

$$\tau(z) = \bar{\tau}[1 - \frac{cosh(\kappa z)}{cosh(\kappa L/2)}], 0 \leq z \leq L/2$$

eqn. 3.6

As such, the derivative of the interlayer stress quickly follows as:

$$\dot{\tau}(z) = \dot{\bar{\tau}}[1 - \frac{cosh(\kappa z)}{cosh(\kappa L/2)}], 0 \leq z \leq L/2$$

eqn. 3.7

Finally, the interlayer shear stress τ is proportional to the interlayer shear ν, with the proportionality constant depending on the interlayer modulus and thickness.

$$\nu(z) = \frac{\tau(z)}{k}$$

eqn. 3.8

The time derivative of ν is identical to the product of the shear rate and interlayer thickness, with the shear rate being the quantity of intrest..

$$\dot{\nu}(z) = \dot{\gamma}t = \frac{\dot{\tau}(z)}{k}$$

eqn. 3.9

This relates the interlayer shear to the time rate of change over the entire length of the beam. Similar to static interlayer shear deformation, the shear rate is at a maximum at the edges of the beam, and falls sharply to zero as the center is approached. For STF interlayers, the edges will always thicken first, with more and more of the beam slowly following with increasing deformation rate. However, it will be impossible to thicken the entire sample for any finite velocity. As such, only a fraction of the total interlayer will be actively involved in the mechanics of the beam.

Armed with this relationship, it will now be possible to calculate the effects of including a viscous interlayer material. Viscous flow and wall stresses can now

directly be calculated, which relate respectively to the viscous losses and changes in elastic properties of the beam during a dynamic deformation.

3.2 Selection of Important Parameters

Construction of the computer models began by selecting which, of the multitude of forces acting on the system, to include. Of clear importance were the elastic forces, which will dominate at low deformation rates, and the viscous drag produced as the interlayer deforms under shear, which was anticipated to become significant at higher velocities. Because the system inherently involved variable deformation rates, inertial effects were also considered for inclusion. Indeed, artifacts in some of the early experimental results were initially erroneously attributed to inertia. All other forces were excluded, such as the thickening energy attributed to STFs, and other non-idealities, such as squeeze flow, etc.

Upon closer examination, it was discovered that inertial forces were negligible for the system under consideration. The force due to inertia is a direct result from constantly changing the kinetic energy of the system. Over the distance of the displacement, the beam must be accelerated from rest, through a maximum velocity, and then brought back to rest at the maximum displacement. Assuming a sinusoidal velocity profile, it can be shown that maximum velocity is root 3 times the average velocity. Further, this velocity maximum occurs halfway through the displacement. Average velocity can be readily calculated from twice the displacement and the frequency. Mass can be found from the beam densities, and dimensions of the various layers in the composite beam. Assuming the entire mass of the beam is accelerated to the maximum velocity, a quick estimate of the kinetic energy can be obtained. In reality, however, the

entirety of the beam does not move during the bend. The ends are supported and have zero velocity; only the middle of the beam obtains the maximum velocity. In order to find the true result, the shape of the bent beam must be known, and so Dr. Gillespie's model is once again employed. The shape of the bent beam can be found by integrating the shear in the interlayer along the length of the beam, and results in a shape that ranges from a hyperbola for stiff beams, to a triangle in the extreme of a infinitely long beam. The average of the square of the shape yields a multiplier factor to correct the previously found inertial force to one more relevant to the system. It was found, that for the systems studied on the DMA, with average velocities below 0.3m/s (0.15m/s in the later experiments), that the inertial forces were negligible compared to the elastic forces for the decoupled beams, and as such, inertia was not included in the model.

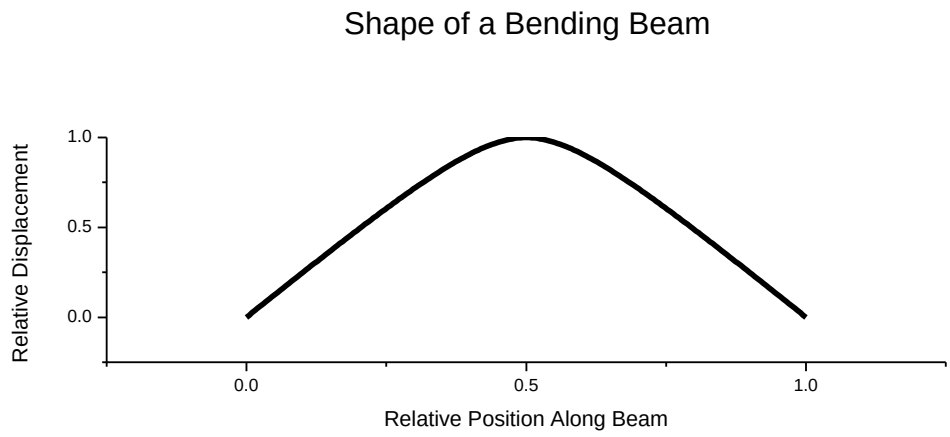

Figure 3.1- Possible shape of a bending beam. Exact shapes will vary depending upon the beam's unique parameters.

3.3 Modeling STF Behavior

In order to improve the validity of the results, an improved model was obtained by fitting various functions to experimental results obtained on a rheometer. Because of the discontinuous nature of the viscosity, it was decided to model the fluid in a piecewise fashion, rather than with a single function. It was found that the shear thinning regime was fit extremely well by a modified logistic function. For the shear thickening portion, several models were tried, with varying degrees of success. First was an exponential function, which was found to have a poor fit. Second was a linear function, with a good fit, and a reasonable extrapolated region in which viscosity continued to increase with increasing shear rate. Finally, a second logistic function was tried, which resulted in a good fit, but a ceiling in the extrapolated region many orders of magnitude lower than STFs are able to achieve. As such, the linear fit was found to

model the system the best, and the Logistic-Linear model adopted for the simulations. Below is the final piecewise model selected.

$$\eta^* = \begin{cases} a_2 + \frac{a_1 - a_2}{1 + \frac{\dot{\gamma}}{x_0}^p} : \dot{\gamma} \leq 17s^{-1} \\ m\dot{\gamma} + b : \dot{\gamma} > 17s^{-1} \end{cases}$$

eqn. 3.10

	a1	**a2**	**x0**	**P**
Logistic	561.87512	2.21573	1.64403E-4	.64708
	m	**B**		
Linear	13.47074	-239.78174		

Table 3.1-Parameters for the piecewise fit of the complex viscosity.

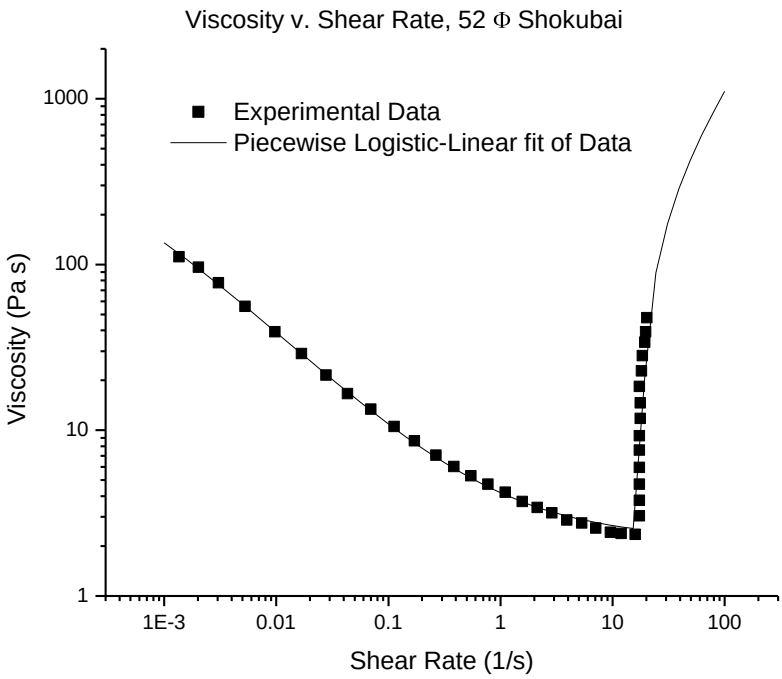

Figure 3.2-Piecewise fitting of STF complex viscosity.

3.4 Uncoupled Model

The initial model developed assumed that the viscous interlayer had an infinitesimal elastic modulus. As such, the two beams would remain essentially decoupled during the entirety of the bend, regardless of the viscous interactions with the interlayer. While not a comprehensive model of the system, it did have the advantage of being simple to program, with no iterations required. Code logic is as follows:

1. Beam deformation rate is found from the frequency (varying) and the displacement (constant).

2. The deformation rate is transformed into a shear rate (as a function of position in the beam) for each of the 100 discretized points in the beam. This shear rate is combined with the fluid viscosity to find the shear forces along the beam.
3. The deformation rate is also used to find the shear displacement rate.
4. Combining the shear force with the shear displacement rate yields the power dissipation due to the viscous interlayer. Summing up theses values along the length of the beam and dividing by the deformation rate relates this to an increase in the force required to bend the beams.

A quick examination of the results indicated that this simplified model was flawed. At low deformation rates, the model predicted reasonable results, but at the higher velocities, the predicted modulus of the beam structure quickly became unreasonable, exceeding 10^{13} pascals for even the lowest viscosity interlayers. This simplified model clearly does not capture the high velocity data of the system, and as such a more involved model is necessary. The implications of this simplified model are important nonetheless. In particular, it implies that the viscous forces quickly reach a level where they are causing a significant amount drag on the faces of the beams, resisting the shear deformation. This force is very similar to the shear force exerted by the elastic adherand in Dr. Gillespie's model. As such, even though the viscous interlayer is assumed to have no elastic modulus, it will have an apparent elastic modulus arising from its viscosity. This will have the result of decreasing the viscous losses in the system by reducing the interlayer shear rate, at the cost of increasing the

elastic modulus of system and increasing stiffness by forcing the beams to behave more like a coupled system.

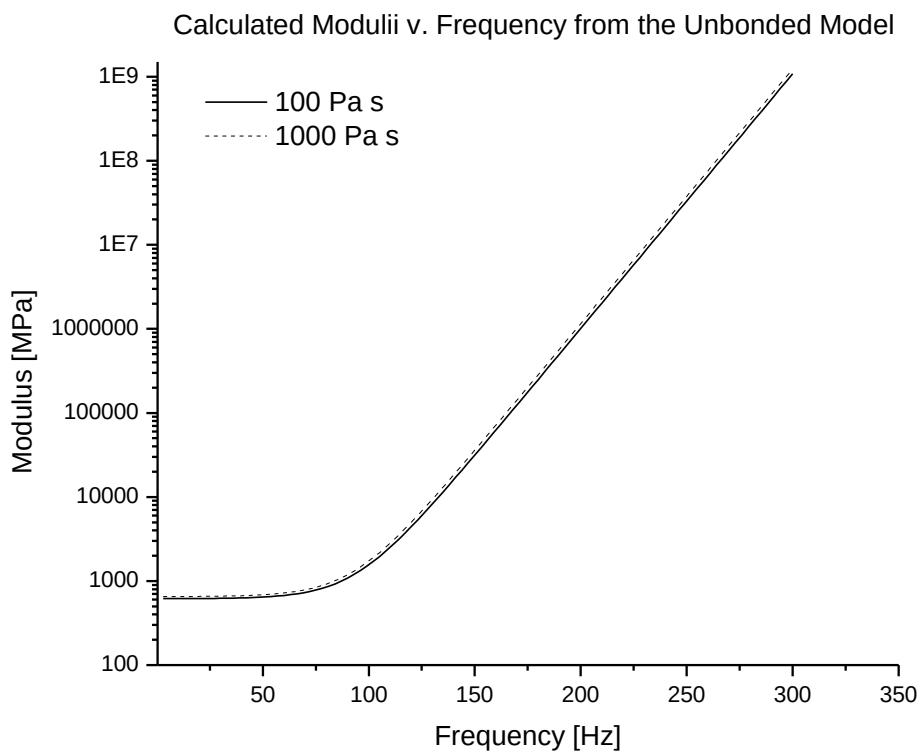

Figure 3.3-Select beam modulii calculated with the un-bonded model. Note that at high frequencies the model returns absurdly high modulii.

3.5 Coupled Model

The coupled model is very similar to the uncoupled one, except with the inclusion of iterative loops to match the apparent interlayer elastic modulus to the shear

rate. Further, this model also accounts for the varying velocity profile throughout the bend. The original code logic was modified as follows:

An arbitrary start value is selected for the apparent elastic interlayer modulus. For STF calculations, a starting value of viscosity is also selected. In the Newtonian model, this is supplied by the user prior to performing any calculations.

Due to the relationships between the interlayer viscosity, the interfacial stresses, and the apparent interlayer modulus, two nested iterations were required to converge the model. The first inner iteration ensures that, for a constant value of viscosity, the interfacial shear stresses are consistent between the apparent interlayer modulus and the viscous flow. Once stable, the resulting shear rate is used to iterate to the next value of viscosity. The inner loop is then run again, until all three values are in agreement.

For approximately 100 unique points through the bend, the following is done:

1. An initial iterative loop is entered. This loop is built around viscosity, and holds this value constant while the value for the apparent elastic modulus is stabilized. This prevents the program from returning NaN when trying to simultaneously vary viscosity and interlayer modulus. This master loop does not exist in the Newtonian version, where viscosity does not change.
2. Key values for the next slave loop are rest, and the slave loop entered.
3. In the nested loop, the value of the current interlayer modulus is used to calculate the interlayer shear and shear rate.

4. This value of shear rate is used to calculate the interface shear stresses on the beams.
5. This shear stress is reduced to an apparent interlayer modulus.
6. The current value of interlayer modulus and the calculated value are compared. If they agree to a tolerance of 10^-4, the loop is exited. Otherwise, the current value is replaced with the calculated value, and the loop repeated until the values agree.
7. The current shear rates returned from the slave loop are then used to calculate the viscosity of the interlayer STF. Once again, this new value is compared with the old value. If they agree within the tolerance, the calculation is complete, otherwise, the new value is again feed into the slave loop.
8. Once all of the calculated values have stabilized, important values are collected from and displayed as a function of the current deflection. These include the Elastic Forces, the "Non-Conservative" (viscous) forces, total force, shear displacement, shear rate, apparent interlayer modulus, the "Dynamic Modulus" (the apparent interlayer modulus based on shear rate rather than shear, which can be more informative), and the interlayer viscosity.
9. Finally, the above values are used to calculated both the Storage and Loss modulii for the beam system as a function of displacement velocity.

When running these models to predict the results for a real experiment, it is important to have an accurate value of the viscosity, as these values can have an enormous effect on the final results. For the Newtonian viscosity standards, this is as trivial as reading the manufacturer supplied viscosity value. However, for the STFs, the computer has to be able to accurately select the correct value for the variety of shear rates during the beam's bend. Initially, a power law tuned to take off at around the same shear rate as the STF was used.

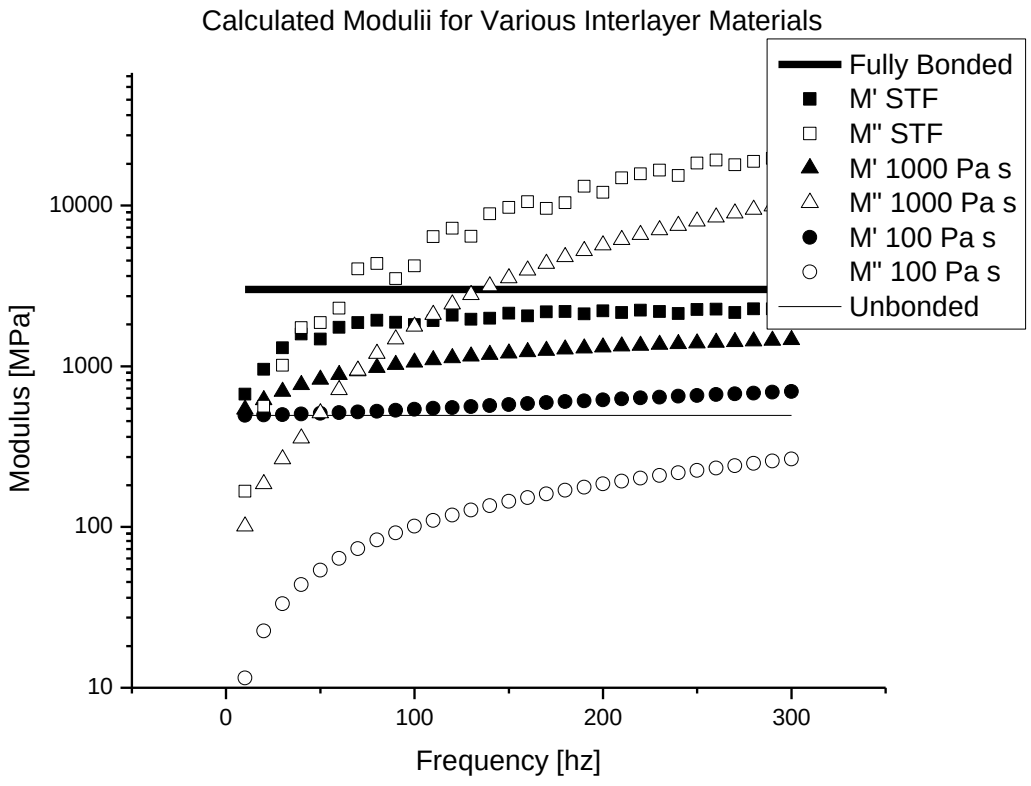

Figure 3.4-Modulli for various viscous interlayers, as calculated by the coupled simulation.

The final result from coupled model follows intuition much better than the original, uncoupled model. Instead of having the viscous forces quickly overwhelm the elastic interactions, and obtain absurd levels, the viscous forces remain close to the values of the elastic forces. While it is possible for the viscous forces to dominate, this only occurs for the thickest fluids, such as the STF, and even when it does occur, the viscous interactions remain within reasonable bounds. In essence, the coupled model shows that viscous interlayer sandwich beam actually reacts to a dynamic force in such a way as to increase its compliance, while attempting to minimize the viscous forces experienced in the interlayer.

The model also predicts that even for the thickest samples, the coupling effect is incomplete. This can be interpreted as a balance by the interface stressed produced by the liquid. If the stresses were so high as to completely arrest the relative motion between the beams, there would be no flow in the viscous interlayer, and subsequently the force bonding the beams together would disappear. Some level of relative motion between the beams is required to maintain the bonding effect, even for the most viscous interlayers.

Finally, the model predicts the interesting result that for STF interlayer beams, the viscous forces will actually dominate at high deformation rates. At sufficiently high velocities, the response of the beam actually becomes liquid like. If extrapolated to the velocities expected in a ballistic impact, this model would predict the majority of the beams response would be in viscous dissipation of the impact energy, rather than elastic deformation of the beam.

Chapter 4

DMA EXPERIMENTS

4.1 The Mettler Toledo DMA/SDTA861^{e}

Laboratory experiments were performed on a Mettler Toledo DMA/SDTA861^{e}. Dynamic Mechanical Analyzers (DMA) are typically used to find a materials modulus as a function of temperature. For example, a DMA will often be used to find the glass transition temperature of a material. Mettler Toledo's DMA is a precision instrument consisting of an actuator, a force and displacement transducer, and an oven. The oven can ohmicly heat the sample to 500 ^{o}C or cool it using liquid nitrogen to -150 ^{o}C, and maintain the set temperature to within 0.5K. The force transducer will read forces as low as 5mN through 40N, with a sensitivity of 1mN. Total displacement is 3.2mm (+/- 1.6mm) with a sensitivity of 5nm. Finally, frequency can vary between 0.001 and 1000Hz (.001 to 300Hz for most geometries).

Figure 4.1-The DMA.

The DMA offers a wide choice of sample geometries, as well as control parameters, each useful for experiments and samples. Geometries include fixtures for shear (liquids), compression (solids), as well as 3 point bend, with other geometries available. Experimental variables available include time, which may be useful if the sample is a curing resin, temperature (for values like the glass transition temperature), and others such as frequency and displacement. With some creative programming, other variables can also be available, such as clamping force, or multiple variables may be varied at once.

The 3 point bend fixture was used exclusively for the laboratory experiments. Geometric constraints from the sample fixture limited sample size to a length between 30mm and 100mm, a width of about 15mm and a thickness of approximately 5mm. Further, mechanical restraints on the machine limit the frequency to 300Hz. As such, the sample geometry chosen for the experiments was 60mm (50 between supports) x 10mm. The additional 10mm of overhang proved sufficient to prevent the beam from slipping of the supports during the experiment. Thickness was variable based on the thickness of the beam material, but varied between about 0.75mm and 3mm.

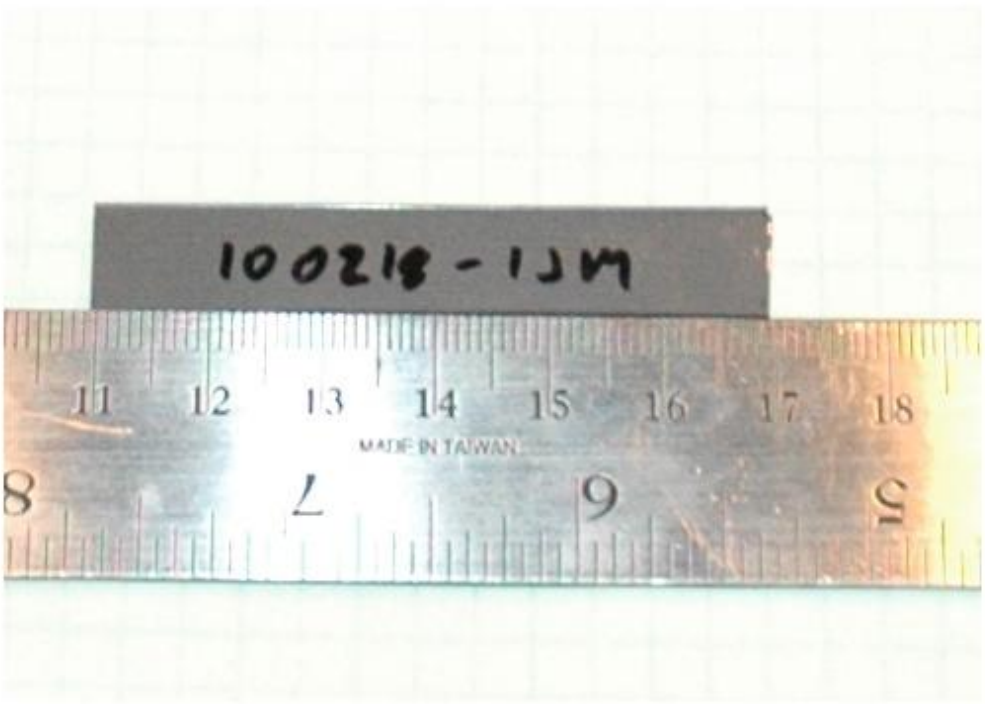

Figure 4.2-A beam sample from the DMA.

Programming the DMA is a relatively simple task, mostly due to Mettler's proprietary graphical user interface. The STARe software interface allows the operator to simultaneously define experimental parameters, control and collect data from several instruments, and analyze data. The software breaks experiments into various segments, during which different experimental parameters are varied. For composite beam experiments described here, the entire experiment consists of a single segment, during which either frequency or displacement, and by extension thereof the displacement velocity, is varied. The other variable would be set to either 500 micrometers, or 150 hertz, respectively. The other parameter of importance is the offset, which defines the clamping force exerted by the instrument (all the more important due to the inverted support system). A narrow range is required for a successful experiment. 105% offset was used in the experiments, as this fell in the sweet spot between reliable results and maximum displacement velocity. The Fast DMA option was not used for any of the experiments. This option allows the instrument to collect data at an increased rate at the expense of precision. For the composite beams used in this study, this loss in precision resulted in significant systematic error in the data.

4.2 Sample Preparation

Beams were formed from 6,6 Nylon sheets purchased from McMaster Carr. Two types were used, a thinner fiber reinforced sample, about 0.75mm thick, and a thicker plain sample, approximately 1.5mm thick. Beams were cut from the thinner samples using a simple utility knife and straight edge. After measuring out the appropriate width, the straight edge was clamped to the beam stock. The utility knife was then dragged along the straight edge several times, scoring the stock and ensuring a

clean straight sample. After a sufficiently deep groove was formed, the straight edge was removed, and the knife dragged along the groove several more times until the sample was severed from the stock. Attempting to cut the ticker beams with the knife proved much too labor intensive, and so a band or hack saw was employed. The cut was made slowly and deliberately in order to ensure as straight an edge as possible.

Once the beams were fabricated, a thin piece of plastic shim stock, between 3 mil and 10 mil (depending on the sample, with many more thicknesses readily available) were tacked lengthwise along the edges of one beam using a contact adhesive such as adhesive photo spray or contact cement. This plastic shim "sets" the interlayer gap, and prevents squeeze flow or other forces from changing the interlayer geometry. The shims are cut as thin as feasibly possible, generally on the order of 1mm. Other methods were also tried, such as large spherical particles or thin gauge wire, both of which were found to be inferior. After a few minutes, once the cement had cured, the interlayer fluid was liberally spread across the surface of the beam and spacers, and the second beam placed on top. The entire beam was then gently pressed together, to squeeze out any excess material, and a micrometer run along the length to confirm the total beam thickness was correct.

Interlayer materials ranged from simple air, essentially two beams placed on top of each other and allowed to freely slide against one another, through concentrated STF suspensions. Other Newtonian interlayer materials were thick silicone oils, typically a mixture of different length chains of poly-dimethylsiloxane, produced by manufactures such as Union Carbide and Brookfield scientific as viscosity standards. The dynamic viscosity of these liquids was between 100,000 and 7,000,000 centipoise, making theses extremely thick, gooey, and not particularly free flowing fluids. Fluids of

this viscosity were required to generate significant interlayer responses during the testing. Before attaching the upper beam, the sample was placed under vacuum for two hours, in order to remove any air bubbles in the interlayer material.

The STF used during the testing was a suspension of mono-disperse spherical 450nm, surface treated silica particles produced by the Shokubai Corporation, dispersed in 200MW polyethylene glycol (PEG). This particle system was chosen because it is extremely well characterized. Samples were prepared in the typical fashion. A 52 volume percent suspension was selected, as this sample exhibits one of the highest and most aggressive viscosity increases, which will in turn result in the most obvious trends in the beam bending data. Samples were prepared by weighing out the corresponding masses of particles and PEG, and placed both into a single plastic sample jar. This jar was then sealed and placed on a roll mixer overnight, allowing the particles to disperse themselves throughout the PEG.

4.3 Issues Encountered

The beams prepared in the above manner are not particularly stiff, especially when compared to a monolithic beam of the same proportions. The DMA used in the study, powered by a 40 Newton actuator, was designed for samples that were many times stiffer than these beams, which take much less than a Newton to deform by 500 micrometers. As such, there was a significant technical challenge in coaxing useful data from the instrument. Among the roadblocks that needed to be overcome were several issues relating to the sample clamping and resulting creep, displacement issues due to exceeding the instruments operating limitations, as well as erroneous data arising from negative phase angles.

In a traditional 3 point bend experiment, the beam is resting on the supports, and the load descends to meet the sample from above. In such a geometry, gravity acts to keep the beam and the supports in contact. However, the Mettler DMA does not adhere to this traditional geometry, but rather uses its inverse. In the DMA, the supports are above the beam sample, and the actuator arm has to both clamp the beam to the supports and deform the sample. As a result, at minimum displacement the actuator must still be slightly deforming the beam, in order to supply enough force positively overcome the weight of the sample. If insufficient force is applied, or more accurately the zero displacement of the actuator is too low to maintain contact between the beam and the supports, a gap will appear between one of the supports and the beam. Under these conditions, over the course of the displacement, the beam will initially swing upward, during which the unsupported end will build momentum. Then, as it abruptly impacts the support (in which the load sensor is housed), a large, short duration impulse appears as the free end of the beam is decelerated to zero velocity. The impulse results in erroneous peak force data, which ultimately translates to calculated modulii many orders of magnitude too high. This can result in calculated modulus in excess of 10^14, which exceeds that of diamond. This vibration produced impulse becomes more prominent at lower frequencies. At high frequency, the beam does not have enough time to fall off of the supports, and as a result the effect is minimal or non-existent. Only at actuator velocities comparable to or less than those attained through gravity can the beam disengage from the supports enough to have a significant effect. In order to prevent this phenomenon, an offset exceeding 100% must be specified in the experimental method.

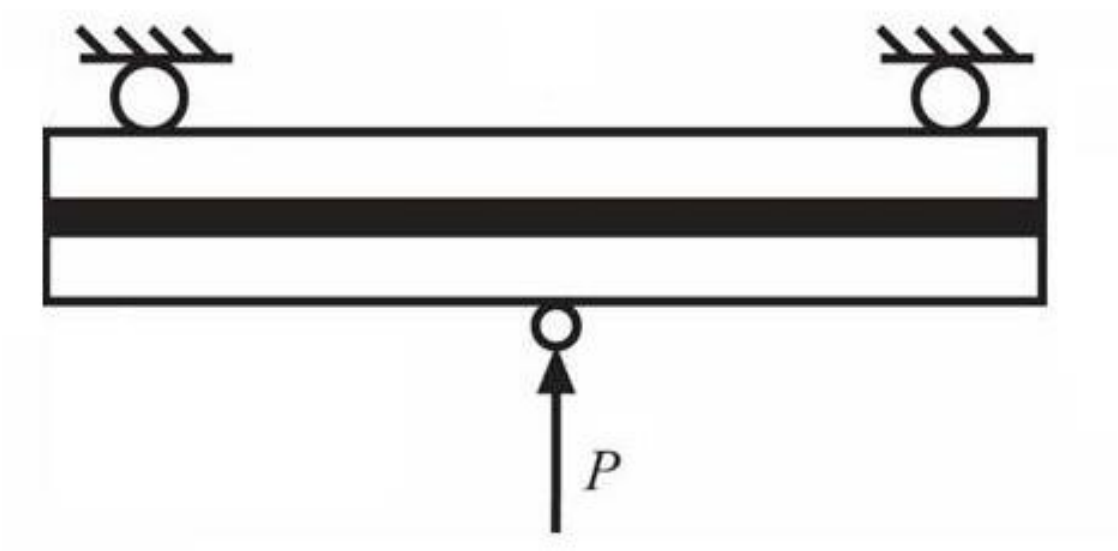

Figure 4.3- DMA's three point bend geometry. The distance between supports is 50mm, and the sample is about 3mm thick

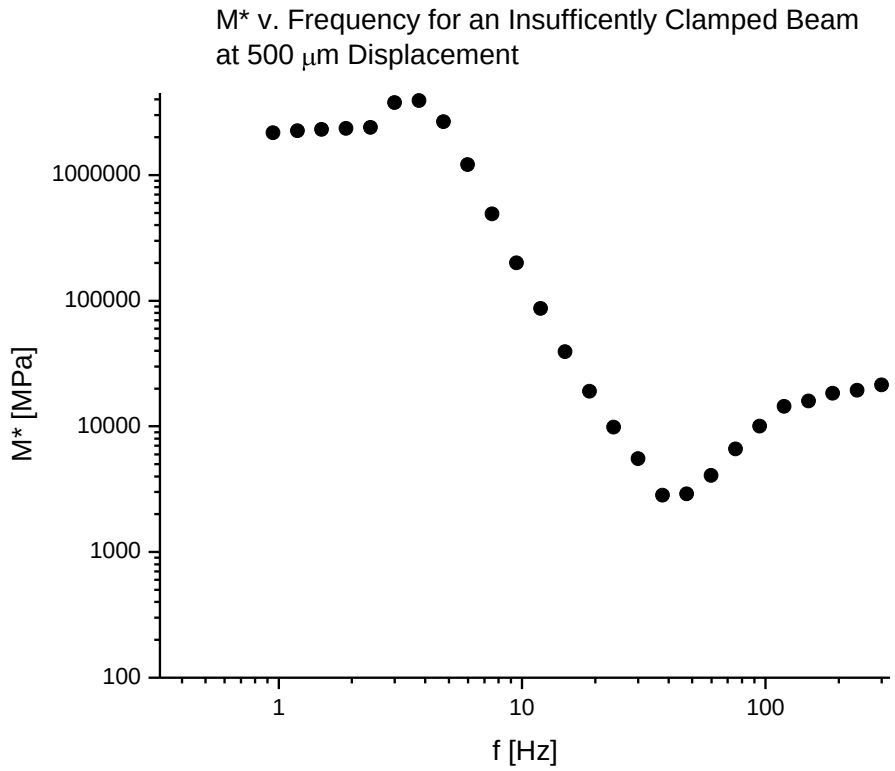

Figure 4.4-Plot of M* for a poorly clamped beam. Notice the enormous modulus under 10 hz of up to 3000 GPa. The elastic modulus of diamond is around 1200 GPa.

Problems also arise when the percent offset is set too high. The plastic beams used in the experiments have two characteristics that make them susceptible to high offsets. First, they are plastic in nature, and thus slowly stretch while under load. As such, maintaining the clamping force will require the actuator to continually move upward. This, coupled with the low stiffness of the beams results in a situation where an already significant offset must constantly grow in order to meet the experimental

criteria. This becomes an issue particularly during high displacements, where the offset is the greatest. Because the instrument has a max displacement of only 1600 microns, the sum of the experimental displacement and the offset displacement cannot exceed this number. As a digital safeguard, the DMA will not allow the overall displacement to exceed this value, and so as the offset approaches 1500 microns, the experimental displacement will fall to around 40 microns, as opposed to the 400 or 500 as specified in the method.

When the overall actuator displacement peaks, the instrument automatically truncates the displacement, preferentially preserves the offset, and does not trip an error. It will continue to perform the experiment with the shortened displacement, as if nothing were wrong. As a result, the only way to know if the displacement is correct is for the operator to carefully examine the reported displacement and confirm that the values agree with those specified in the method. In most displacement experiments, the actuator will not max out until near the end of the experiment, with the rest of the experiment producing useful information. In frequency ramped experiments, in many cases the displacement was orders of magnitude off of the specified value for the entire experiment, resulting in entire runs of relatively useless data.

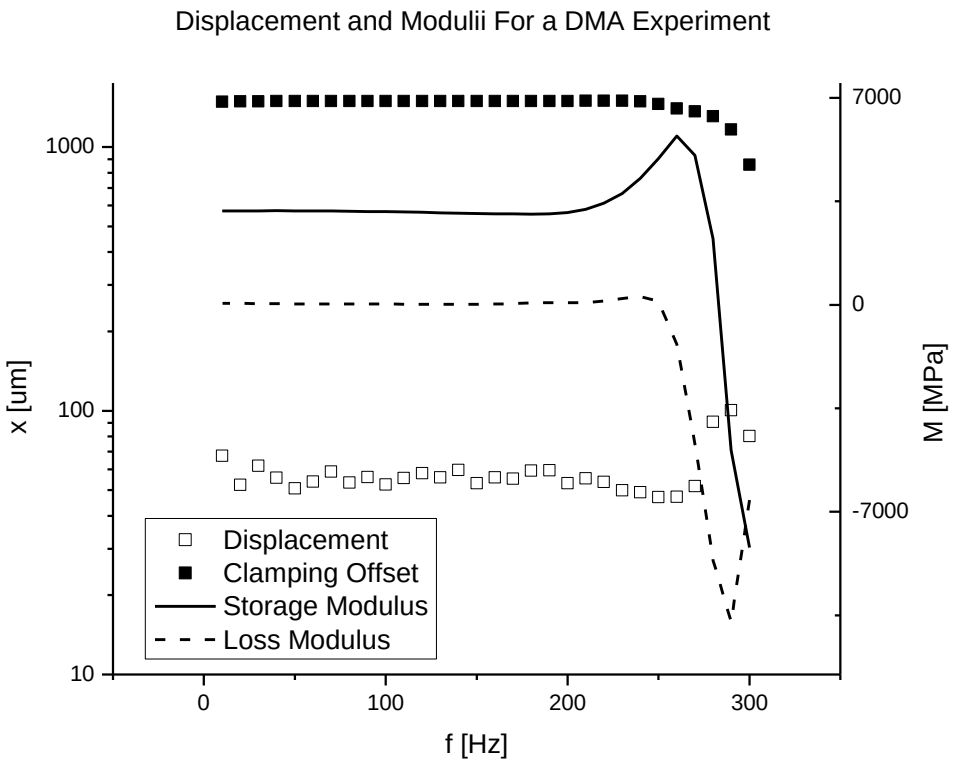

Figure 4.5-Example of a run where the maximum displacement was exceeded. 500µm of displacement was specified, but less than 100µm obtained. Modulii were still calculated, regardless, based on the 100µm displacement.

Another issue that arose was negative modulii. The instrument functions by inputing a sinusoidal wave into the actuator arm, causing a stress in the sample and measuring the force amplitude, as well as strain. Among its various outputs is the phase angle, defined by the phase difference between peaks in the periodic input stress and resulting periodic strain in the sample. This value is always positive, meaning the sample responds only after the input stimulus, and generally small. However, under some conditions, such as when approaching the resonance frequency of the sample, the

peaks may appear to switch, resulting in a strain curve that 'leads' the stress wave. This results in a negative phase angle, where the sample is pulling the actuator, rather than the actuator pushing the sample.

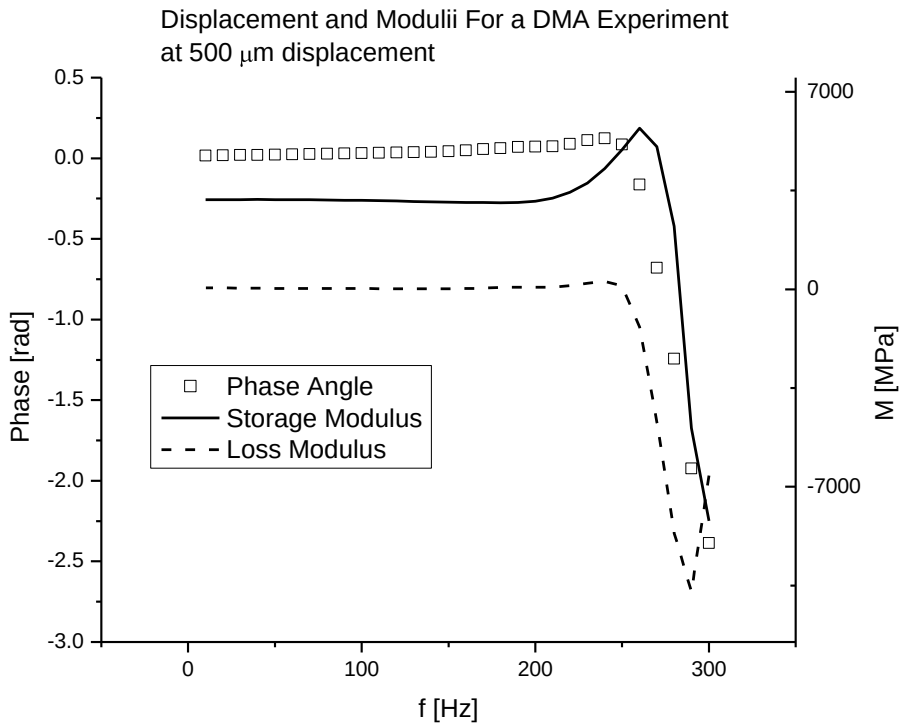

Figure 4.6-Comparison of phase angle and modulii. As the phase angle becomes negative, so do the storage and loss modulli.

Compounding the issue is that the default value reported by the instrument is not the storage and loss modulii, which will become negative as the phase angle becomes negative, but the arithmetic mean of the two, which remains positive regardless of the phase angle. Typically, the mean will grow rapidly as the phase angle becomes more negative. Similar to the displacement, no errors are tripped when the

phase becomes negative. Without the full picture, this value alone can be easily mistaken for valid data. Since the phase angle becomes negative at the higher frequencies, it was initially postulated that the phenomenon was due to increased viscous or inertial forces as a result of the high velocities. Upon closer inspection of the phase angle, however, it was realized that the tail end of the curve was merely an artifact in the stress/strain data.

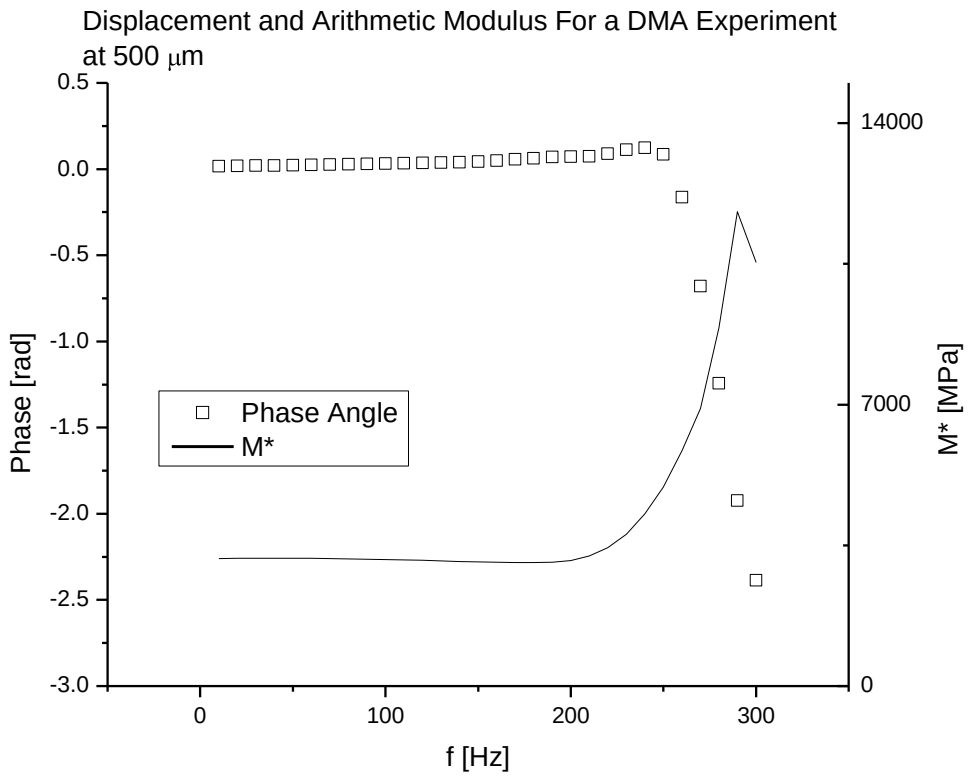

Figure 4.7-Comparison of the arithmetic modulus and phase angle. As the phase angle becomes negative, M* remains positive.

Ultimately, any data collected on the DMA can not be simply taken as reported. It must be approached with intelligence and engineering knowledge. All aspects of the data must be analyzed, to ensure that the instrument is both performing the experiment programmed, and is also generating useful data. It is a powerful tool, but can be difficult to use due to various subtleties involved with running highly compliant samples.

4.4 Comparison of Results

The DMA results show that the viscosity of the interlayer material plays a quantifiable role in the final dynamic properties of the sandwich beam. The STF interlayer has a storage modulus that is about 20% greater than that of the viscosity standard. Similarly, the STF interlayer generates the highest loss modulus, which is nearly twice that of the viscosity standard.

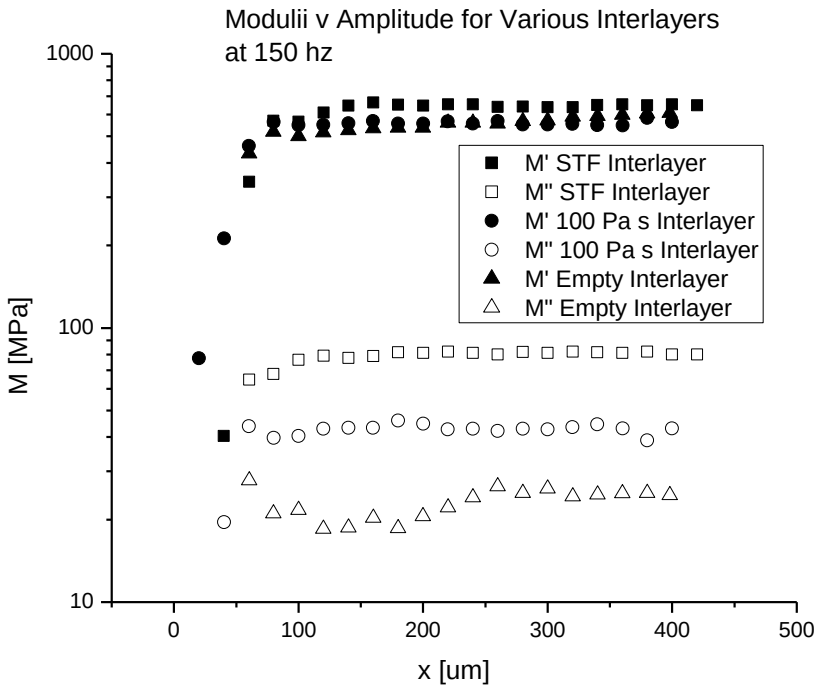

Figure 4.8-Effect of interlayer on beam modulli.

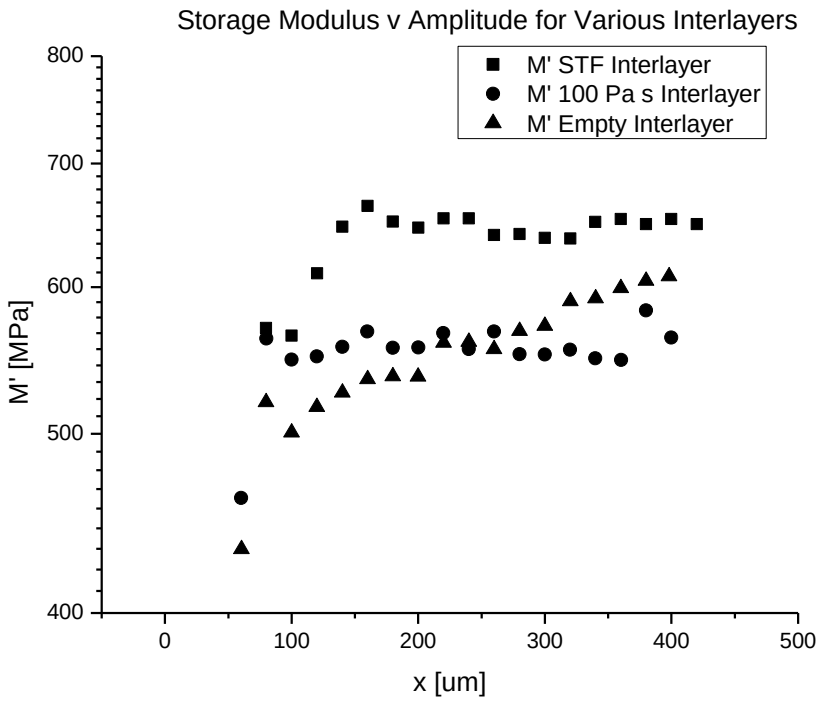

Figure 4.9-Improved view of storage modulii v amplitude.

When compared with the values obtained from the computer simulations, the results are mixed. The model correctly predicted that a viscous Newtonian interlayer with a viscosity of approximately 100 Pascal seconds would cause little, if any discernable increases in elastic modulus for displacements up to 0.5mm at 150 hz. Further, the value for the loss modulus was within about a factor of 2 over this entire range. This lends credibility to the computer model and the math backing it, since it is able to predict with reasonable tolerance, the minimum viscosity required to affect the net beam properties.

While being able to predict the minimum for the coupling effect, the model did not perfectly describe the data. In particular it overpredicted both the elastic and

viscous modulii for the STF interlayer. The model calculated that the storage modulus would grow with increasing deformation velocity until leveling off around 2000 MPa (66% of the monolithic beams modulus). The value recorded with the DMA also increases to a plateau, but levels off at the much lower value of about 700 MPa. This is still larger than the uncoupled beams, but only about 1/3 of the value anticipated in the model.

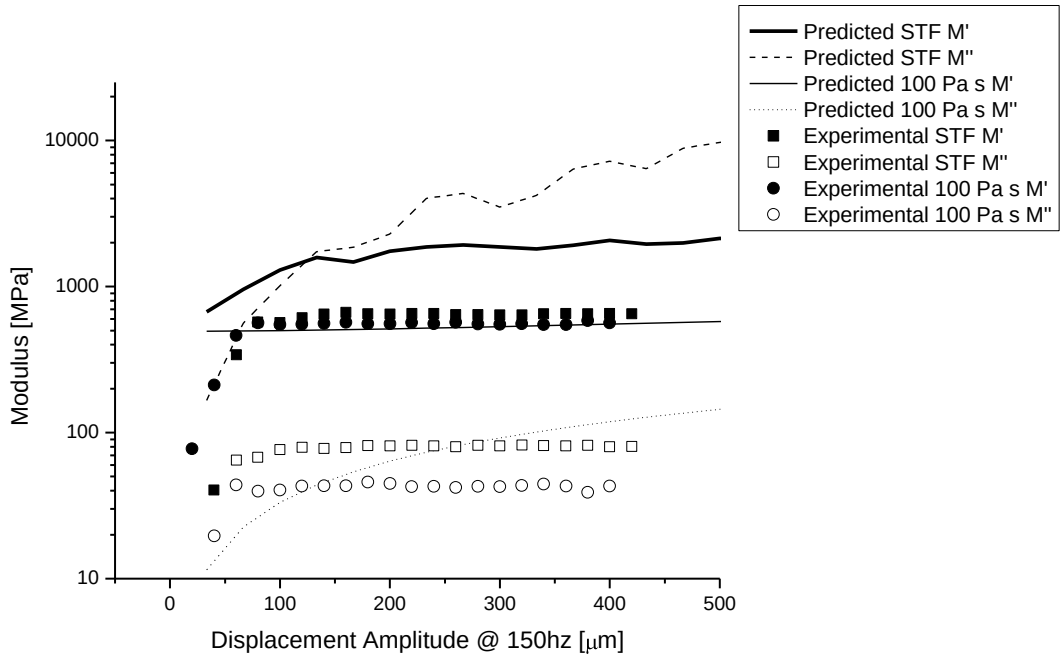

Figure 4.10-Overlay of the computer simulation and experimental results.

The loss modulus of the STF interlayer is similar to that of the storage modulus in that the computer simulation overpredicts its value. The computer model finds that the loss modulus will increase in magnitude over several decades, and quickly

become greater than the elastic storage modulus. However, the experimental data show the opposite. The loss modulus, while significantly higher than that of the viscosity standard, remained at low values. In particular, it leveled off at a value approximately an order of magnitude lower than the storage modulus, instead of exceeding it by a similar margin.

The mismatch between the computer simulation and the experimental results is possibly due to a rheological phenomenon known as slip that is unaccounted for in the simulation. When the STF used in the experiment undergoes its thickening transition, it transforms from a thick sticky liquid to a hard solid-like material with a high degree of cohesion but little adhesion. If a small drop is spilled on a table top, it is extremely easy to peal the STF off of the surface with a spatula or gloved finger nail, yielding a small pebble-like bead of STF and a table top with only a minimal amount of residue. This property means that if enough shear stress is applied to the interlayer, the STF could delaminate from one of the beam surfaces, or slip. This would result in two separate beams with net modulii that are only slightly greater than the uncoupled case, instead of drastically larger.

If slip is in fact occurring, it can be minimized or eliminated by roughening the surfaces of the beams, with a sand blaster or emery paper. This will provide both an increase in surface area to bond to, as well as peaks and troughs which form physical barriers that the solid-like STF cannot penetrate.

Chapter 5

THE TOWER OF POWER

5.1 Specifications

Building upon the information gathered from the DMA experiments, as well as the computer modeling, a final experiment has been designed, but has yet to be performed, for the Tower of Power. The Tower is a new, large, high energy drop tower run by the University of Delaware Center for Composite Materials. It has a maximum drop height of 12 feet, and a maximum mass of 2000 pounds, replicating the kinetic energy of modern assault rifles, but at a much slower rate, leading to a more controlled experiment.

The Tower of Power is highly instrumented. Unlike most other drop towers, which may have one or two force sensors, the Tower has a plethora of sensors, measuring the load on both the impacter and sample to determine not only the total force, but also torque that occurs during the experiment. Magnetic strips along the length of the rail precisely determine the position and velocity of the sled at all times. Mounting brackets are also present, to allow inclusion of high-speed videography, and laser rangefinders. The extensive instrumentation package allows for an increased insight into the dynamic processes occurring during the impact.

While both the DMA and Tower use the same 3 point bend geometry, the two instruments do not run the same experiment. The DMA studies beams subject to high frequency, low velocity deformation. Further, it subjects the samples to a periodic

and well defined stress wave. The Tower subjects its sample to a single, high velocity, high energy impact, for the duration of a single deflection. The test is much more violent, and subjects the samples to much higher stress and strain waves. Data is collected over the whole deformation of the beam, rather than just at the peaks, allowing a closer look at the mechanics during the bend, rather than just generalized over the entire period. Ultimately, the data collected during such a full scale test will offer a deeper and more complete picture than any available from a DMA experiment.

5.2 Computer Modeling

Modeling this system was once again performed in MATLAB, using similar computational techniques as for the DMA. However, the computation was simplified by neglecting any transverse waves propagating through the beam due to impulse loading, and neglecting the kinetic energy in the beam. Two nylon beams measuring a meter long, 20cm wide, and 2cm thick, and joined with an interlayer of negligible thickness will be approximately 9 kg (assuming a density of 1.1 g/cm^3), or about 1% of the mass of the 900kg sled. Understanding that not all of the mass of the beam is actually moving during the bend, and that most of the mass is moving much slower than the sled, the beam will contribute an effective mass to the system of less than 1%, and as such has been neglected. Similarly, the energy obtained by the falling sled after impact is also ignored. Finally, the viscosity of the STF is assumed constant along the length of the beam, despite local shear rates that may be much smaller than the average. This value is taken to be the viscosity associated with the shear rate at the tips of the beams.

Code logic is almost identical to the DMA models, and follows the kinetic energy of the sled as it is converted to other forms of energy, namely the elastic potential of the deformed beam, and the energy lost through viscous dissipation:

1. An Impact velocity is derived from the sled mass and drop height.
2. This velocity is used in an iterative to calculate the beam and interlayer parameters, based on a specified viscosity.
3. The interlayer shear is returned from (2.) and used to find the STF viscosity under these conditions. The viscosity is then iterated around this value and returned to (2.). This process is repeated until a stable viscosity is found.
4. The elastic and viscous forces on the beam returned from (2.) and used to calculate the energy required for a small increase in displacement.
5. These energies are used to deincrement the kinetic energy of the system, and a new velocity found. The code then returns to step (3.), and continues until all of the kinetic energy is converted.

5.3 Results

The model suggests that under these higher velocity, high shear deformations, the STF interlayer between the two beams will nearly instantaneously thicken to its near solid-like state. Effectively, this prevents the two beams from sliding against each other; as evidence the viscous loss is nearly zero, despite the enormous viscosity. Only as the beam begins to slow and the STF relax does the shear rate fall enough for any significant viscous losses. During the peak deformation, the interaction

shifts between storing energy in the beams, and viscously dissipating it as heat. Essentially, as the beam slows the STF begins to relax and flow, subsequently allowing the nylon beams to relax.

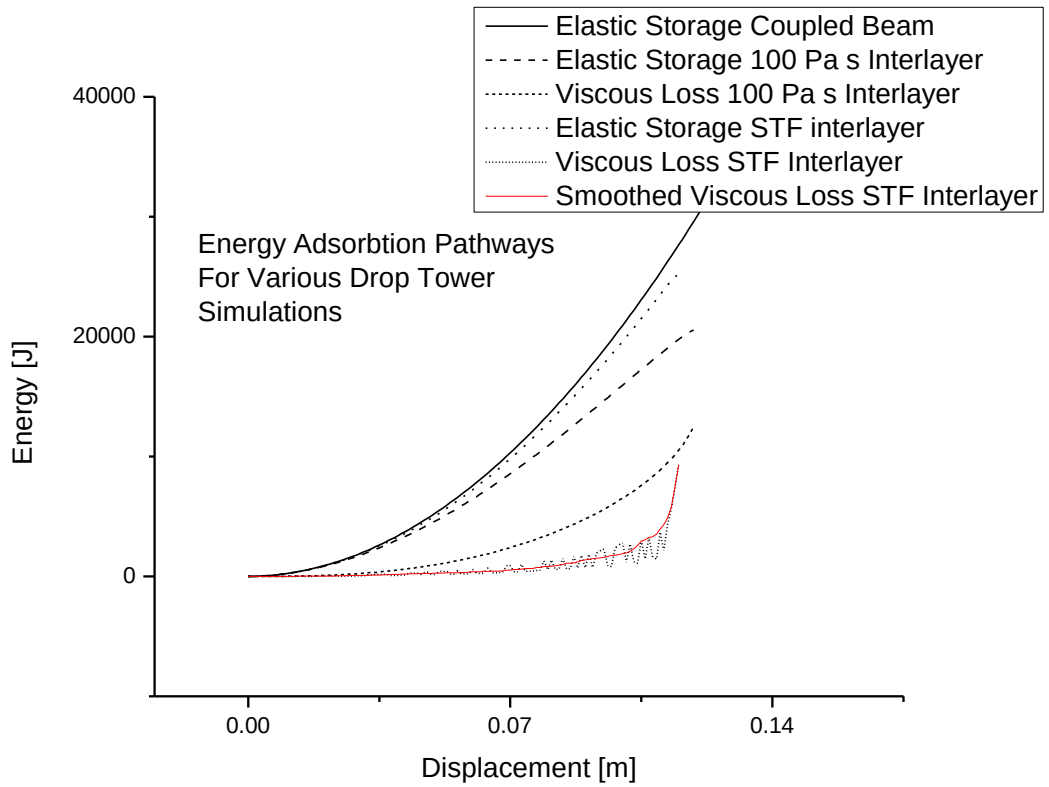

Figure 5.1-Adsorbed energy v displacement for several drop tower simulations.

Beam Type	Max Displacement (m)	Elastic Storage (% energy)	Viscous Loss (% energy)
Uncoupled	0.251	100	0
Fully Bonded	0.125	100	0
100 Pa s	0.119	62.3	37.7
1000 Pa s	0.115	77.6	32.4
STF	0.115	73.0	37.0

Table 5.1-Comparison of displacements and energy adsorption modes for various beam interlayers.

Ultimately, the model predicts that a sandwich beam with a thin interlayer of STF will reduce the maximum deflection of the beam structure by almost 50%, when compared with a similar system in which the beams are free to slide along each other. Further, the elastic forces are almost identical to that in the fully bonded simulation. This suggests that for highly viscous interlayers, the predominant role of the interlayer material is not the removal of energy through viscous dissipation as predicted in the DMA model, but rather to bind together the two beams and increase the elastic forces presented by the system as a whole. Due to the high velocity dependence of this binding force, eventually the beams will become decoupled towards the end of the deflection. It is only as the elastic forces diminish, that the viscous interactions begin to become important, resulting in an overall dissipation of kinetic energy and a maximum displacement that is actually slightly smaller than a comparable elastically bound beam with a high modulus interlayer.

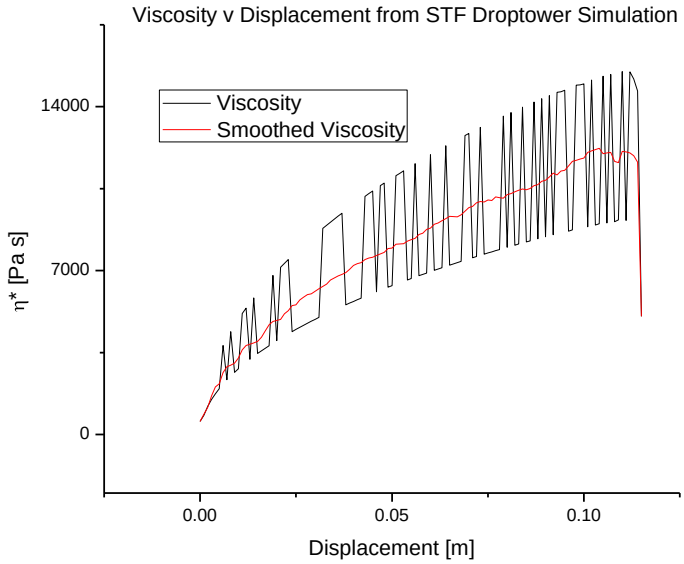

Figure 5.2-Viscosity v displacement as returned from the simulation. It is very noisy, but follows a definite trend. Note the significant decrease at the extreme deformations.

The deviation between the two computer models can be attributed to the velocity profile used in each. Because of the sinusoidal nature of the velocity profile in the DMA, where the beam is initially at rest and accelerated through two maximums in velocity, after each of which it is again returned to rest, the beam spends much less time on average at full shear, and more time accelerating through periods of relatively low shear, where the viscous forces are insufficient to bind the beams together. As such, it suggests that viscous dissipation is an extremely important mechanic in the function of the beam, to the extent that for extremely viscous interlayers, the viscous forces will actually dominate. However, the Tower simulations offer evidence to the contrary. The high impulse loading of the beam essentially negates viscous terms during the initial

acceleration. It is only as the system begins to slow that viscous flow becomes important, and even then they are still secondary to the elastic forces from the beams. Ultimately, the models suggest that an experiment performed on the Tower of Power would in fact present a more realistic situation, and hence produce more useful information. The two techniques, while very similar, are in fact performing two different experiments, and the results must be taken into consideration as such.

Chapter 6

CONCLUSION

Several computer models covering various distinct deformation rate profiles were developed to study the dynamic bending behavior of beam sandwiches with a viscous interlayer when subject to a three point bend. One of the models was compared to experimental values, with mixed results, while the other was used to design a second experiment.

It was found that velocity profile, as well as its magnitude, have an enormous effect on the sandwich beams. Deformation velocities that are bound to a sinusoidal profile tend to emphasize the viscous interactions over the elastic. Profiles similar to those that result from a projectile emphasize the elastic forces instead.

Further, interlayers with a viscosity below a critical value were found to have a negligible effect on the final properties of the composite beam. This critical viscosity is determined by both the deformation rate, as well as the geometry of the interlayer.

Comparison between the models and experimental data demonstrated that the models were able to correctly predict the value of the critical viscosity below which the beam properties would be essentially unaltered. However, it drastically overpredicted the effect of a shear thickening interlayer. This overprediction has been attributed to slip in the interlayer, but further experimentation is required to confirm this hypothesis.

The computer simulations have suggested that a shear thickening interlayer can be integrated into a composite armor system and simultaneously provide a high armor rating while protecting the system from mobility damage. Such a system could improve soldier survivability while simplifying logistics and maintenance programs. However, more experimentation both with the small scale DMA, as well as large scale ballistic simulations such as the Tower of Power will be required to ultimately confirm these findings.

REFRENCES

[1] Alfredsson, K. S., T. A. Bogetti, A. Carlsson, J. W. Gillespie Jr, and A. Yiournas. "Flexure of Beams with an Interlayer -- Symmetric Beams with Orthotropic Adherends." *Journal of Mechanics of Materials and Structures* 3.1 (2008): 45-62.

[2] Curiel, T., and G. Fernlund. "Deformation and Stress Build-up in Bi-material Beam Specimens with a Curing FM300 Adhesive Interalayer." *Composites: Part A* 39 (2008): 252-61.

[3] Daniel, J., D. Melo, and D. W. Radford. "Viscoelastic Properties of PEEK-IM7 Related to Temperature." *Journal of Reinforced Plastics and Composites* 25.5 (2005): 545-56.

[4] Davila, C. G., and T-K Chen. "Advanced Modeling Strategies for Teh Analysis of Tile-Reinforced Composite Armor." *Applied Composite Materials* 7 (2000): 51-68.

[5] Decker, M. J., C. J. Halbach, C. H. Nam, N. J. Wagner, and E. D. Wetzel. "Stab Resistance of Shear Thickening Fluid (STF)-Treated Fabrics." *Composites Science and Technology* 67 (2006): 565-78.

[6] Fischer, C., A. Bennani, E. Jacquelin, and J-A E. Manson. "Structural Dampening of Model Sandwich Structures Using Tailored Shear Thickening Fluid Compositions." *Smart Materials and Structures* 19 (2010): 1-7.

[7] Fischer, C., S. A. Braun, P-E Bourban, V. Michaud, C J G. Plummer, and J-A E. Manson. "Dynamic Properties of Sandwich Structures with Integrated Shear-Thickening Fluids." *Smart Materials and Structures* 15 (2006): 1467-475.

[8] Kalman, D. P., and N. J. Wagner. "Microstructure of Shear-Thickening Concentrated Suspensions Determined by Flow-USANS." *Rheologica Acta* 48 (2009): 897-908.

[9] Kalman, D. P., R. L. Merrill, N. J. Wagner, and E. D. Wetzel. "Effect of Particle Hardness on the Penetration Behavior of Fabrics Intercalated with Dry Particles and Concentrated Particle-Fluid Suspensions." *Applied Materials & Interfaces* 1.11 (2009): 2602-612.

[10] Kirkwood, J. E., K. M. Kirkwood, Y. S. Lee, R. G. Egres, N. J. Wagner, and E. D. Wetzel. "Yarn Pull-Out as a Mechanism for Dissipating Ballistic Impact Energy in Kevlar KM-2 Fabric Part 2: Predicting Ballistic Performance." *Textile Research Journal* 74.11 (2004): 939-48.

[11] Kirkwood, K. M., J. E. Kirkwood, Y. S. Lee, R. G. Egres, N. J. Wagner, and E. D. Wetzel. "Yarn Pull-Out as a Mechanism for Dissipating Ballistic Impact Energy in Kevlar KM-2 Fabric Part 1: Quasi-Static Characterization of Yarn Pull-Out." *Textile Research Journal* 74.10 (2004): 920-28.

[12] Lee, Y. S., E. D. Wetzel, and N. J. Wagner. "The Ballistic Impact Characteristics of Kevlar Woven Fabrics Impregnated with a Colloidal Shear Thickening Fluid." *Journal of Materials Science* 38 (2003): 2825-833.

[13] Mahfuz, H., F. Clements, V. Rangari, V. Dhanak, and G. Beamson. "Enhanced Stab Resistance of Armor Composites with Functionalized Silica Nanoparticles." *Journal of Applied Physics* 105 (2009).

[14] Mahdi, S., and J. W. Gillespie. "Finite Element Analysis of Tile-Reinfoced Composite Structural Armor Subjected to Bending Loads." *Composites: Part B* 35 (2004): 57-71.

[15] *Shear Thickening Fluid (STF) Fabric*. University of Delawar Center for Composite Materials. Web. 11 May 2010. <http://www.ccm.udel.edu/STF/index.html>.

[16] Wagner, N. J., and J. F. Brady. "Shear Thickening in Colloidal Dispersions." *Physics Today* (2009): 27-32.

Appendix A

NOMENCLATURE

$C \equiv \frac{x}{P}$	Compliance of the sandwich beam
x	Bending displacement of beam
v	Displacement velocity
P	Force exerted on beam
$\bar{V}$	Total shear force transmitted by beam
$C_{bt} = \frac{\frac{L^3}{32Ebh^3}}{1+\frac{3}{2}\frac{t}{h}+(\frac{t}{h})^2}$	Compliance according to ordinary beam theory
L	Length of beam
b	Width of beam
h	Thickness of adherends
t	Interlayer thickness
E	Adherend modulus
G	Interlayer modulus
$A \equiv Ebh$	
$D \equiv Ebh^3$	
$\kappa \equiv \sqrt{\frac{8G}{Eht}[1 + \frac{3}{2}\frac{t}{h} + \frac{3}{4}(\frac{t}{h})^2]}$	
$\bar{\tau}$	Maximum interlayer shear stress
$\dot{\bar{\tau}}$	Time derivative of maximum interlayer shear stress
z	Position along length of beam
$\tau(z)$	Shear stress along length of beam
$\dot{\tau}(z)$	Time derivative of shear stress
$k \equiv \frac{G}{t}$	
ν	Interlayer shear
$\dot{\nu}$	Time derivative of interlayer shear
$\dot{\gamma}$	Shear rate
η^*	Complex Viscosity
M'	Storage Modulus
M''	Loss Modulus
$M^* \equiv \sqrt{M'^2 + M''^2}$	Arithemetic mean of Modulii
f	Frequency